Published in final edited form as:
Vision Res. 2009 February ; 49(4): 479–489. doi:10.1016/j.visres.2008.12.009.

Early defects in photoreceptor outer segment morphogenesis in zebrafish *ift57*, *ift88* and *ift172* Intraflagellar Transport mutants

Sujita Sukumaran and **Brian D. Perkins***
Department of Biology, Texas A&M University, College Station, TX 77843

Abstract

Intraflagellar Transport (IFT) refers to a highly conserved process occurring in eukaryotic ciliated structures. In vertebrate photoreceptors, IFT mediates protein trafficking to the outer segments. The IFT particle is a multi-subunit complex and mutations in many individual components causes photoreceptor defects. In zebrafish, mutations in the *ift57*, *ift88* and *ift172* genes result in retinal degeneration by 5 days post fertilization (dpf). Although the effects of these mutations on photoreceptor survival have been described, early developmental morphogenesis remains poorly understood. We used transmission electron microscopy and immunohistochemistry to examine these mutants at 60, 72, and 96 hours post fertilization (hpf) and describe early photoreceptor morphogenesis defects.

Keywords

Retina; Photoreceptor; Intraflagellar transport; Connecting cilium; Outer Segment

Introduction

Vertebrate photoreceptors have a unique morphology consisting of an inner and outer segment linked by a connecting cilium. The tip of the outer segment is shed on a daily basis and is phagocytosed by the retinal pigment epithelium (Young, 1967). To replace this lost material, the photoreceptor inner segments contain cellular organelles that continuously supply material for outer segment maintenance. The connecting cilium that bridges the inner and outer segments possesses a 9+0 microtubule structure (Fawcett & Porter, 1954). The connecting cilium can be classified as having three distinct regions; an upper axoneme that is continuous with the outer segment, a middle part that is surrounded by surface membrane and a lower portion that penetrates into the inner segment and attaches to the basal body, which is a centriole-like structure that anchors the connecting cilium in retinas (De Robertis, 1956).

In the initial stage of photoreceptor development, a cilium projects from a bulge of protoplasm of the inner segment (De Robertis, 1956). The apical end of the primitive cilium continues to enlarge and accumulates “morphogenetic material” that consists of short pieces of tubules and vesicles. Primitive disk membranes then replace the morphogenetic material and align transverse to the surface membrane. These morphogenetic observations show that the outer

* Corresponding Author: Brian D. Perkins, Department of Biology, 3258 TAMU, Texas A&M University, College Station, TX 77843, Ph: 979-845-6505, Fax: 979-845-2891, Email: E-mail: bperkins@mail.bio.tamu.edu.

segment is formed as a result of differentiation of the distal portion of the primitive cilia. The basal part of the cilium however, remains undifferentiated and is continuous with the basal body (De Robertis, 1956, Horst, Johnson & Besharse, 1990). The outer segment hence requires transport of ciliary components, such as membranes and microtubules, and proteins required for structure and phototransduction (Mendez, Lem, Simon & Chen, 2003, Perkins, Fadool & Dowling, 2004, Peterson, Tam, Moritz, Shelamer, Dugger, McDowell, Hargrave, Papermaster & Smith, 2003).

Protein trafficking via the connecting cilium is mediated by a process known as Intraflagellar Transport (IFT). IFT was discovered in the unicellular biflagellate organism, *Chlamydomonas*, as the movement of granule like particles along the length of the flagella (Kozminski, Johnson, Forscher & Rosenbaum, 1993). In adult photoreceptors, IFT proteins localize to the inner segment, basal body region and along the length of the outer segment axoneme (Luby-Phelps, Fogerty, Baker, Pazour & Besharse, 2008, Pazour, Baker, Deane, Cole, Dickert, Rosenbaum, Witman & Besharse, 2002). In vertebrates, mutations in the IFT particle affect several tissues such as photoreceptors, kidney, nodal cilia, olfactory neurons and hair cells (Pazour & Rosenbaum, 2002, Tsujikawa & Malicki, 2004).

Mutations in three specific IFT subunits, *ift57, ift88* and *ift172*, have profound effects on the retina (Gross & Perkins, 2008, Krock & Perkins, 2008, Pazour et al., 2002, Tsujikawa & Malicki, 2004). The mouse null mutants *hippi*, *flexo* and *wimple*, which encode *ift57*, *ift88*, and *ift172*, respectively, cause defects in left-right patterning and Shh signaling. These mutations result in embryonic lethality prior to retinal differentiation, which has prevented analysis of photoreceptor phenotypes in these mutants (Houde, Dickinson, Houtzager, Cullum, Montpetit, Metzler, Simpson, Roy, Hayden, Hoodless & Nicholson, 2006, Huangfu, Liu, Rakeman, Murcia, Niswander & Anderson, 2003). However, a hypomorphic mutation of *Ift88* in mice, the $Ift88^{Tg737Rpw}$ allele, is viable and shows gradual loss of outer segments followed by photoreceptor degeneration (Pazour et al., 2002). We previously found that *ift57* mutant zebrafish had short outer segments whereas *ift88* and *ift172* mutants completely lack outer segments at 5 days post fertilization (dpf) (Gross, Perkins, Amsterdam, Egana, Darland, Matsui, Sciascia, Hopkins & Dowling, 2005, Krock & Perkins, 2008). It is unclear, however, whether the initial stages of outer segment growth, such as primitive cilium projection or assembly of "morphogenetic material," are also affected in zebrafish *ift57* mutants. Detailed ultrastructural analyses of *ift88* and *ift172* mutants at early timepoints have not been described and it is unclear if loss of these subunits prevents all aspects of outer segment formation or if early morphological differentiation occurs but the nascent outer segment rapidly degenerates.

To address these questions, we analyzed the three IFT mutants at 60 hpf, 72 hpf, and 96 hpf, by transmission electron microscopy and immunohistochemistry to chart the progress of photoreceptor morphogenesis and examine the distribution of proteins destined for the outer segment. Our results indicated that outer segments initially formed normally in a subset of *ift57* mutant photoreceptors but further maturation was inhibited. In contrast, outer segment formation was never observed *ift88* and *ift172* mutants. These results reveal subtle differences between various IFT mutants and suggest different factors are necessary for initiating outer segment formation.

Materials and Methods

Zebrafish care and maintenance

The zebrafish *oval* locus encodes *ift88* and *oval* mutants contain a nonsense mutation resulting in a premature stop codon identified in exon 11 (Tsujikawa and Malicki, 2004). The *ift88* null mutant zebrafish were a gift from Jarema Malicki. *ift57* and *ift172* mutants were obtained from

a retroviral insertional mutagenesis screen (Gross et al., 2005). All fish were maintained in accordance with established procedures (Westerfield, 1995).

Transmission Electron Microscopy

All mutants and wild type fish were fixed at 60 hpf, 72 hpf and 96 hpf in 1% paraformaldehyde, 2.5% glutaraldehyde and 1% tannic acid. Embryos were processed with osmium tetroxide as secondary fixative, followed by a dehydration series in ethanol and infiltrated with epoxy resin as previously described (Krock & Perkins, 2008). Transverse sections (0.1 μm in thickness) obtained at the optic nerve region were post stained with 2% uranyl acetate and Reynolds lead citrate. Images were collected on a JEOL 1200EX transmission electron microscope and whole images were adjusted for brightness and contrast with Adobe Photoshop.

Immunohistochemistry

Embryos were fixed in 4% paraformaldehyde at the designated timepoints and processed as described previously (Perkins, Nicholas, Baye, Link & Dowling, 2005). The dilution of primary antibodies used were as follows: monoclonal 1D1 (1:100), monoclonal ZPR1 (1:200), monoclonal anti-acetylated tubulin (Sigma 1:500), rabbit polyclonal anti-IFT52 (1:3000) and polyclonal anti-IFT88 (1:5000) (Krock & Perkins, 2008). Fluorescent labeled anti-mouse and anti-rabbit secondary antibodies were used at 1:500 dilutions (Invitrogen). DAPI (1:400) was used as a counter stain. Images were collected using an AxioImager fitted with an ApoTome attachment (Zeiss) and processed with Adobe Photoshop.

SDS Page and Western Blotting

Embryo heads were removed at 60, 72 and 96 hpf and lysis buffer (PBS + 1% Triton + 5mM EDTA) was added at 3 μl per head. The lysate was homogenized and sonicated prior to dilution in 4X SDS buffer. The solution was boiled at 95 °C for 5 minutes and centrifuged for 10 minutes at 13,200 rpm. Samples were loaded on 12% Tris-HCl ready gels (Bio-Rad). Proteins were transferred onto a PVDF membrane and labeled with appropriate antibodies. The primary antibody dilutions used are as follows: Rabbit anti-IFT88 (1:3000), Rabbit anti-IFT52 (1:1500) and mouse anti-acetylated tubulin (1:10,000) (Sigma). Super signal west femto maximum sensitivity substrate (Thermo scientific) and Immunostar HRP substrate Kit (Bio-Rad) were used as secondary antibodies for detection of IFT antibodies and acetylated tubulin, respectively.

Results

We analyzed the zebrafish *ift57*$^{hi3417/curly}$, *ift88*$^{tz288b/oval}$, and *ift172*$^{hi2211/moe}$ mutant alleles, which we will refer to as the *ift57*, *ift88*, and *ift172* mutants, respectively. The *ift57* and *ift172* mutations resulted from retroviral insertions into exons near the 5′ end of the gene (Amsterdam, Burgess, Golling, Chen, Sun, Townsend, Farrington, Haldi & Hopkins, 1999), whereas the *ift88* mutation is a nonsense mutation generated by ENU mutagenesis (Malicki, Neuhauss, Schier, Solnica-Krezel, Stemple, Stainier, Abdelilah, Zwartkruis, Rangini & Driever, 1996). These mutants were described as having defects in ciliated sensory neurons and pronephric cilia (Gross et al., 2005, Sun, Amsterdam, Pazour, Cole, Miller & Hopkins, 2004, Tsujikawa & Malicki, 2004).

Zebrafish carrying homozygous mutations in the *ift57*, *ift88* and *ift172* genes exhibit photoreceptor cell death (Gross et al., 2005, Krock & Perkins, 2008, Tsujikawa & Malicki, 2004). The 60 hpf timepoint was chosen because the first photoreceptors begin to differentiate at 50-54 hpf (Hu & Easter, 1999, Raymond, Barthel & Curran, 1995, Raymond, Barthel, Rounsifer, Sullivan & Knight, 1993) and the first outer segments can be readily observed at

60 hpf (Schmitt & Dowling, 1999). Analysis at 72 and 96 hpf were used to determine any defects in outer segment development as wild type retinas mature (Nawrocki, 1985).

We used transmission electron microscopy to analyze early photoreceptor anatomy and outer segment structure at 60 hpf in all three IFT mutants (Fig. 1). Transmission electron microscopic study of wild type photoreceptor architecture at 60 and 72 hpf has been previously described in detail (Schmitt & Dowling, 1999). Consistent with these previous studies, we observed similar features in wild type embryos at 60 hpf, such as large numbers of mitochondria in the inner segments and sporadic outer segments in the ventral patch (Figs. 1A-C). Wild type photoreceptor outer segments were short but contained loosely stacked disk membranes and connecting cilia were observed (Fig. 1B). We occasionally observed primary cilia extended from the apical surface of the inner segment in central and dorsal regions of the retina, where morphogenesis was just beginning (Fig. 1C). We found outer segments in *ift57* mutants at this timepoint (Figs. 1D-F). These outer segments contained regularly stacked disk membranes and did not differ significantly from wild type. Statistical analysis using a student t-test between wild type and *ift57* mutant embryos revealed no difference in outer segment length at this timepoint (Fig. 4A; $p>0.05$). In contrast, we never observed organized structures resembling an outer segment in *ift88* or *ift172* mutants (Figs. 1G-L). Interestingly, we occasionally observed disorganized membrane material deep within the inner segment and below the mitochondria (Fig. 1K). In both *ift88* and *ift172* mutants, we also observed disorganized membranes in the apical region of the inner segments (Figs. 1H, I, L). However, connecting cilia were not detected in *ift88* or *ift172* mutants and these disorganized structures did not resemble outer segments. On rare occasions, we observed parallel arrays of membrane along the lateral membrane of all IFT mutants, which were similar to the ones observed along the lateral membrane for *ift88* mutants at 88 hpf (Tsujikawa & Malicki, 2004).

We next examined the IFT mutants at 72 hpf to look for elongation of outer segments and further photoreceptor differentiation. Wild type larvae at 72 hpf showed an increase in number of outer segments and the disk membranes became more tightly stacked and organized (Figs. 2A-C). Surprisingly, we did not observe an increase in outer segment length between 60 hpf and 72 hpf in wild type embryos (Figs. 4A, C). At 72 hpf, a small number outer segments were still observed in *ift57* mutants (Figs. 2D-F). Overall, *ift57* mutants had 88% fewer outer segments than the wild type siblings (Fig. 4B). However, the existing outer segments showed no difference in length from the wild type (Fig. 4C; $p>0.05$). Connecting cilia were observed in several photoreceptors in both wild type and *ift57* mutants (Fig. 2; arrows). Outer segments and ciliary projections were still absent in *ift88* and *ift172* mutant embryos at this timepoint, suggesting that outer segment formation and ciliogenesis failed to occur and was not simply delayed (Figs. 2C-D). We continued to observe disorganized membranous structures in the *ift88* and *ift172* mutants (Fig. 2; arrowheads). These structures were deeper within the inner segment and often seen below the mitochondria (Figs. 2I, K; arrowheads). In one image, a centriole was observed deep within the inner segment and away from the apical surface where the basal body would normally be found (Fig. 2L; asterisk).

At 96 hpf, the outer segments of both rod and cone photoreceptors can be observed throughout the retina and photoreceptor nuclei exhibit tiering within the outer nuclear layer (Figs. 3A, E). At 96 hpf, *ift57* mutants were much shorter (Figs. 3B, F), although disk stacking appeared normal, similar to our previous observations (Krock & Perkins, 2008). The number of outer segments observed in *ift57* mutants was reduced by 90% when compared to wild type larvae (Fig. 4D) and pyknotic nuclei and acellular holes were observed, indicating cell death (Krock & Perkins, 2008); data not shown). In wild type larvae, outer segment length increased significantly between 72 hpf and 96 hpf to almost 4 microns (Fig. 4E). In contrast, *ift57* mutant outer segments did not significantly increase in length and were 38% shorter than wild type outer segments. These data indicate that *ift57* mutant photoreceptors were unable to extend the

outer segments like wild type animals (Fig. 4E). We previously noted that *ift57* mutant photoreceptors were 75% shorter at 96 hpf (Krock & Perkins, 2008). In the previous work, however, outer segment measurements were limited to the ventral retina where photoreceptor differentiation initiates and where the oldest, and therefore largest, photoreceptors reside. In the current analysis, we measured outer segments from both rods and cones throughout the entire retina and we included measurements of outer segments from younger photoreceptors in both wild type and *ift57* mutants. Thus, *ift57* mutant photoreceptors remain shorter than wild type, but ventral photoreceptor outer segments were much shorter than wild type relative to dorsal photoreceptors. Even at this late stage of development, we failed to observe any outer segments in *ift88* and *ift172* mutant embryos (Figs. 3C, D, G, H). Disorganized membranous structures were found at all time points in the three mutants. The loosely arranged stacks could represent membranous material unable to extend from the apical surface and form outer segments, thus leading to toxicity and degeneration of photoreceptors in the mutants. Collectively, these data draw a picture of failed attempts at outer segment morphogenesis in *ift88* and *ift172* mutants and the inability to grow and maintain outer segments in *ift57* mutants, all of which resulted in maturation defects and ultimately premature death.

To complement the TEM data, we performed immunohistochemistry to identify defects in protein trafficking and cell morphology at the three time points. The outer segment defects observed by electron microscopy led us to hypothesize that rhodopsin would be mislocalized to the inner segments of IFT mutants. We stained retinal sections of 60 hpf embryos using 1D1, an antibody against rhodopsin. While rhodopsin mRNA can be observed as early as 50 hpf in wild type embryos (Schmitt & Dowling, 1996), only a limited number of cells were observed with rhodopsin immunoreactivity. Cells staining positive for rhodopsin revealed rhodopsin localization to the outer segment in wild type and *ift57* mutants (Figs. 5A, B), although some mislocalization was also seen in *ift57* mutants. In contrast, both *ift88* and *ift172* mutants exhibited rhodopsin mislocalized to the inner segment and plasma membrane, indicating that protein trafficking was abnormal in these mutants (Figs. 5C, D). We also used zpr1, which is also known as Fret-43 and stains red/green double cones, to investigate cell morphology of mutant cone photoreceptors (Figs 5E-H). Normal cone morphology, as noted by the columnar shape and orderly distribution of cells, was observed in wild type sections, as well as all three IFT mutants. To determine if the trafficking defects observed in IFT mutant rods also occurs in cones, we examined the localization of a cone visual pigment. Blue opsin (BOPS) is expressed in the long single cones of zebrafish (Raymond et al., 1993) and localizes to the outer segment of adults (Vihtelic, Doro & Hyde, 1999). In retinas of 60 hpf wild type animals, BOPS staining localized to the apical inner segment, although some staining remained in the plasma membrane and inner segment (Fig. 5I). In all three IFT mutants, BOPS staining was observed in the apical region of the photoreceptors in a pattern similar to wild type embryos (Figs. 5J-L). As outer segments were very small at 60 hpf in the wild type and *ift57* mutants and not observed in the *ift88* and *ift172* mutants by electron microscopy, we suspected that BOPS staining represents opsin in the apical inner segments, while the nascent outer segments cannot be distinguished at this timepoint.

We next investigated whether loss of individual IFT components affected the localization of other IFT proteins. We used antibodies against the zebrafish IFT52 and IFT88 proteins (Krock & Perkins, 2008) to examine localization of these proteins and co-stained with acetylated tubulin to detect any nascent cilia. At 60 hpf, we observed small foci of immunoreactivity against IFT52 and IFT88 that colocalized with acetylated tubulin in wild type sections (Figs. 5M, Q; arrows). As few photoreceptors have differentiated at this timepoint, we rarely observed more than three or four foci of colocalization in each section. Immunoreactivity against IFT52 and IFT88 was not seen in the three mutants (Figs. 5N-P, R-T). This led us to propose two possibilities; 1) The IFT52 and IFT88 subunits were absent in the mutants or 2) Loss of other IFT components resulted in mislocalization of IFT52 and IFT88 protein and redistribution

throughout the cell such that the concentration of these polypeptides was below the level of detection by immunohistochemistry. Western blot analysis showed that IFT52 was present in all mutants, although at lower levels than observed in wild type embryos (Fig. 6). Similarly, IFT88 was present at reduces levels in *ift57* and *ift172* mutants. We did not detect any IFT88 protein in the *ift88* mutants, consistent with previous results showing oval mutants result from a null allele (Krock & Perkins, 2008, Tsujikawa & Malicki, 2004). The results from western blots suggest that IFT52 and IFT88 could be present in the apical region of the IFT mutants, but at concentrations below the level of detection by immunohistochemistry. To ensure that IFT protein mislocalization did not reflect the inability to position the ciliary apparatus, we used antisera that recognize centrin to determine the location of basal bodies in photoreceptors (Giessl, Pulvermuller, Trojan, Park, Choe, Ernst, Hofmann & Wolfrum, 2004). Small foci of centrin staining were observed in wild type and IFT mutants in the apical inner segment (Figs. 5U-X; arrows). These results suggested that IFT mutants correctly positioned basal bodies at 60 hpf.

Changes in photoreceptor health were first evident by 72 hpf and became more pronounced by 96 hpf. By 72 hpf rhodopsin fully localized to the outer segments of wild type embryos (Fig. 7A). In contrast, rhodopsin was mislocalized and found in both the outer and inner segment region of *ift57* mutants, indicating that protein trafficking was disrupted in these mutants (Fig. 7B). *ift88* and *ift172* mutant embryos showed complete mislocalization of rhodopsin, consistent with the lack of outer segments observed with TEM (Figs. 7C, D). Staining with zpr1 revealed that the cones exhibited early stages of disorganization in all the three mutants as compared to wild type cones (Figs. 7E-H). In wild type sections, blue cone opsin was concentrated at the apical end of photoreceptors, although some mislocalized protein was still seen (Fig. 7I). The *ift57* mutant photoreceptors showed slightly more mislocalization in the plasma membrane and basal regions of the inner segment, whereas *ift88* and *ift172* mutants exhibited strong mislocalization (Figs. 7J-L), which is consistent with previous reports on the zebrafish *ift88* mutant at 3 dpf (Doerre & Malicki, 2002). Antibodies against IFT52 and IFT88 recognized small foci in the basal body region and connecting cilia in wild type photoreceptors (Fig. 7M, Q; arrows). However, we could still not detect these IFT components in any of the IFT mutants at 72 hpf (Figs. 7 N-P & R-T). We performed western blotting at 72 hpf and revealed the presence of IFT52 protein in all three mutants and IFT88 protein in *ift57* and *ift172* mutants (Fig. 8). As protein extracts were obtained from embryo heads rather than isolated retinas, we cannot rule out the possibility that IFT proteins are indeed missing from photoreceptors and the immunoreactivity we observed by western blotting reflected expression in other cell types within the CNS. This seemed unlikely as we observed IFT52 and IFT88 immunoreactivity in the *ift57* mutant photoreceptors at later timepoints when photoreceptors are more mature (see below). In wild type and all IFT mutants, centrin immunoreactivity remained located at the apical part of the inner segment and was often seen just below short ciliary projections in wild type photoreceptors (Figs. 7U-X). The location of centrin staining in the mutants suggests loss of IFT components did not dramatically affect proper positioning of basal bodies but the initial formation of photoreceptor axonemes likely requires the function of *ift88* and *ift172*.

Immunohistochemical analysis at 96 hpf revealed more dramatic changes in photoreceptor structure and protein localization. Staining with 1D1 revealed that rhodopsin remained mislocalized to the inner segment region in *ift88* and *ift172* mutants (Figs. 9A-D). In *ift57* mutants, rhodopsin was mislocalized more to the inner segment region when compared to the earlier time points (Fig. 9B). This result, along with TEM data, supports the idea that *ift57* mutants are unable to maintain outer segments during later development, possibly because of increased rhodopsin mislocalization. Zpr1 labeling showed that the mutant cone photoreceptors acquired a disheveled appearance, suggestive of degeneration due to the lack outer segments (Figs. 9E-H). By this timepoint, BOPS was localized almost exclusively to cone outer segments in wild type animals (Fig. 9I). In contrast, *ift57* mutant cones retained some BOPS in small

outer segments but also showed mislocalization throughout the plasma membrane. In *ift88* and *ift172* mutants BOPS immunoreactivity was seen throughout the inner segment and plasma membrane and no outer segment staining could be found. Antibodies against IFT52 and IFT88 were found localized to the basal body region and connecting cilia in the wild type and *ift57* mutants (Figs. 9M, N, Q, R; arrows). Compared to wild type embryos, the number of photoreceptor cilia was significantly reduced in *ift57* mutants (compare arrows in Figs. 9M-N and 9Q-R), which was consistent with the ultrastructural data showing reduced number of outer segments in the mutant. We again failed to detect IFT52 immunoreactivity in *ift88* mutant zebrafish (Fig. 9S) although very small foci of IFT88 and IFT52 immunoreactivity were occasionally seen scattered throughout the inner segments of *ift172* mutants (Figs. 9P, T). However, western blots from the earlier time points showed that these subunits were expressed in the mutants but could not be detected by immunohistochemistry and we have previously documented that IFT88 and IFT52 are present at 96 hpf (Krock & Perkins, 2008). The *ift88* and *ift172* mutants did not show any acetylated tubulin staining in the area predicted for connecting cilia, strongly suggesting that cilia are absent in these mutants (Figs. 9O, P, S, T, W, X). Finally, centrin immunoreactivity remained predominantly localized to the apical region of the inner segment in wild type and all three IFT mutants (Figs. 9U-X). In *ift172* mutants, some centrin staining was observed deeper within the inner segment (Fig. 9X; arrowheads). Fewer foci of centrin immunoreactivity were observed in *ift88* and *ift172* mutants, which correlated with the loss of photoreceptors.

Discussion

We investigated the progression of photoreceptor morphogenesis in zebrafish *ift57*, *ift88*, and *ift172* mutants. A unique aspect of our study was the examination of mutant photoreceptors at 60 hpf when outer segment morphogenesis first becomes apparent in zebrafish (Schmitt & Dowling, 1999). Previous reports focused largely on photoreceptor survival at 4-5 dpf and none have reported ultrastructural data as early as 60 hpf. Classic electron microscopy studies suggested that vertebrate outer segment formation could be divided into three stages (De Robertis, 1956, De Robertis, 1960). First, a primitive cilium extends from the apical surface of the cell. Second, vesicles and primitive “rod sacs” accumulate at the apical end of the primitive cilium. Third, the membranes undergo remodeling and reorientation to form flattened disks. We propose a fourth stage where outer segment grows and extends into its mature length. Our new data suggest that *ift57* mutants successfully complete the first three stages of outer segment morphogenesis but fail to extend beyond a rudimentary length and subsequently die. Furthermore, we could not find evidence that *ift88* and *ift172* mutant photoreceptors were competent to complete the first stage of extending a primitive cilium (Table 1).

Defects in photoreceptor outer segment formation have been extensively documented for the hypomorphic *Ift88*^{Tg737Rpw} mutant mice (Pazour et al., 2002) and the null *ift88* mutant zebrafish (Doerre & Malicki, 2002, Krock & Perkins, 2008, Tsujikawa & Malicki, 2004). Consistent with previous zebrafish studies, we do not observe ciliary structures in *ift88* mutants at 72 hpf or 96 hpf by either acetylated tubulin staining or ultrastructural analysis. Although cilia and newly forming outer segments were readily observable in wild type embryos, we were unable to detect primitive cilia or loosely aggregated outer segment material in *ift88* mutants at 60 hpf. These results argue that loss of *ift88* totally prevents cilia formation in photoreceptors. Characterization of individual components of the complex has shown that IFT subunits may play different roles in various ciliated tissues of the animal (Gross et al., 2005, Sun et al., 2004, Tsujikawa & Malicki, 2004). Interestingly, *ift88* mutants form sensory cilia in the otic vesicle and nasal epithelium during embryogenesis by 30 hpf, although these cilia are not maintained (Tsujikawa & Malicki, 2004). These results may reflect the contribution of maternal protein as IFT88 was detected at low levels at 48 hpf by western blotting (*Perkins et al., unpublished results*).

Our work also provides the first detailed analysis of how loss of *ift172* affects photoreceptor development. Previous studies demonstrated that zebrafish *ift172* mutants form kidney cysts (Sun et al., 2004) and the *ift172* mutant was found in a screen for eye defects (Gross et al., 2005). Our data shows that loss of *ift172* results in phenotypes that closely resemble, but are distinctive from that of *ift88* mutants. Like the *ift88* mutants, *ift172* mutants lack outer segments at all timepoints examined and photoreceptors rapidly degenerate. At 60 and 72 hpf, however, we frequently observed large accumulations of membranous material within the inner segments of *ift172* mutants. While these loosely aggregated membranes were also seen in *ift88* mutants, they were more prominent in *ift172* mutants. These membranes resembled disorganized disk membranes but no connecting cilia were ever observed and the membranes remained closely associated with mitochondria in the inner segment. These data suggest that *ift172* mutant photoreceptors attempted to assemble outer segment material but failed to extend a ciliary structure to contain this material.

Our results extended our previous analysis of *ift57* mutant photoreceptors (Krock & Perkins, 2008) and further characterize wild type outer segment morphogenesis beyond 60 hpf (Schmitt & Dowling, 1999). When we analyzed photoreceptors at 60 hpf and 72 hpf, we were surprised to find no significant increase in wild type outer segment length. Wild type outer segments do grow rapidly in length from 72 hpf to 96 hpf (Figure 4A). We previously reported that *ift57* mutant photoreceptors have shorter outer segments than wild type. This observation could be explained as a failure to maintain the proper length during maturation or a failure to make a normal ciliary extension at the onset of morphogenesis. Quantification of outer segment lengths revealed no statistical difference between wild type embryos and *ift57* mutants at 60 and 72 hpf (Fig. 4), which supports the former hypothesis. It is only at 96 hpf that the *ift57* mutants are appreciably shorter than wild type. Loss of individual IFT components can also affect the localization and stability of other IFT proteins. As *ift57* mutants form outer segments, the IFT52 and IFT88 proteins localized at or near the cilium. Both IFT52 and IFT88 could not be readily detected by immunohistochemistry in *ift88* and *ift172* mutants. Western blot analysis showed that the IFT52 protein was present in all three mutants at all time points studied, albeit at lower levels. IFT88 was present in only in *ift57* and *ift172* mutants and not in *ift88* mutants confirming that it is a null mutant. These results agree with some data from the analysis of IFT mutants in other species. In *Chlamydomonas*, IFT52 localizes to the distal end of basal body transitional fibers (Deane, Cole, Seeley, Diener & Rosenbaum, 2001). Similar to our results, the *C. elegans* IFT52 ortholog *osm-6* localized normally in *C. elegans che-13* mutants, which affect *ift57* (Haycraft, Schafer, Zhang, Taulman & Yoder, 2003). Interestingly, whereas we demonstrated normal localization of IFT88 in *ift57* mutant photoreceptors, the worm IFT88 protein, *osm-5*, was mislocalized throughout the dendrite and cell body in *che-13* mutants (Haycraft et al., 2003). Furthermore, *osm-5* (IFT88) localized to the apical tip of the transition zone in the *osm-6* (*ift52*) and *osm-1* (*ift172*) mutants (Haycraft, Swoboda, Taulman, Thomas & Yoder, 2001), whereas we could not detect IFT88 protein near the apical region where basal bodies likely form in *ift172* mutants. The experiments in *C. elegans* utilized transgenes expressing IFT-GFP fusion proteins, whereas we utilized immunofluorescence of fixed tissue. The different techniques used to detect IFT protein localization may explain these differing results, as the sensitivity of the immunohistochemistry may potentially be lower than that of an IFT-GFP transgene in worms. Alternatively, the order and composition of IFT particle assembly may differ between sensory cilia in worms and vertebrate photoreceptors. Co-immunoprecipitation assays found that the IFT complex can form in *ift57* mutants but it lacks IFT20 (Krock & Perkins, 2008). In *Chlamydomonas*, it has been shown that there is a decrease in *ift57* and an increase in IFT139 in *Chlamydomonas ift88* mutants (Pazour, Dickert, Vucica, Seeley, Rosenbaum, Witman & Cole, 2000).

Our work conclusively shows that *ift88* and *ift172* have similar roles in photoreceptor development. These subunits serve to initiate outer segment formation in photoreceptors. On

the other hand, *ift57* mutants maintain the initial length they achieve at 60 hpf across all time points implying that *ift57* is required for further growth of the structure. Hence our work provides novel details about *ift57*, *ift88* and *ift172* in early photoreceptor development and show how different subunits of the IFT particle can play different roles in the same vertebrate tissue.

Acknowledgements

We would like to thank Jarema Malicki for providing the *oval*^{tz288b} (*ift88*) mutant line. The authors are grateful to Ann Ellis in the Texas A&M Microscopy Imaging Center for her assistance with transmission electron microscopy. This work was supported by the NEI grant RO1EY017037 (to B.D.P.).

References

Amsterdam A, Burgess S, Golling G, Chen W, Sun Z, Townsend K, Farrington S, Haldi M, Hopkins N. A large-scale insertional mutagenesis screen in zebrafish. Genes Dev 1999;13(20):2713–2724. [PubMed: 10541557]

De Robertis E. Morphogenesis of the Retinal Rods. J Biophysic and Biocehm Cytol 1956;2(4 Suppl): 209–218.

De Robertis E. Some observations on the ultrastructure and morphogenesis of photoreceptors. J Gen Physiol 1960;43(6 Suppl):1–13. [PubMed: 13814989]

Deane JA, Cole DG, Seeley ES, Diener DR, Rosenbaum JL. Localization of intraflagellar transport protein IFT52 identifies basal body transitional fibers as the docking site for IFT particles. Curr Biol 2001;11(20):1586–1590. [PubMed: 11676918]

Doerre G, Malicki J. Genetic analysis of photoreceptor cell development in the zebrafish retina. Mech Dev 2002;110(12):125–138. [PubMed: 11744374]

Fawcett DW, Porter KR. A study of the fine structure of ciliated epithelia. J Morphol 1954;94:221.

Giessl A, Pulvermuller A, Trojan P, Park JH, Choe HW, Ernst OP, Hofmann KP, Wolfrum U. Differential expression and interaction with the visual G-protein transducin of centrin isoforms in mammalian photoreceptor cells. J Biol Chem 2004;279(49):51472–51481. [PubMed: 15347651]

Gross JM, Perkins BD. Zebrafish mutants as models for congenital ocular disorders in humans. Mol Reprod Dev 2008;75(3):547–555. [PubMed: 18058918]

Gross JM, Perkins BD, Amsterdam A, Egana A, Darland T, Matsui JI, Sciascia S, Hopkins N, Dowling JE. Identification of zebrafish insertional mutants with defects in visual system development and function. Genetics 2005;170(1):245–261. [PubMed: 15716491]

Haycraft CJ, Schafer JC, Zhang Q, Taulman PD, Yoder BK. Identification of CHE-13, a novel intraflagellar transport protein required for cilia formation. Exp Cell Res 2003;284(2):251–263. [PubMed: 12651157]

Haycraft CJ, Swoboda P, Taulman PD, Thomas JH, Yoder BK. The C. elegans homolog of the murine cystic kidney disease gene Tg737 functions in a ciliogenic pathway and is disrupted in osm-5 mutant worms. Development 2001;128(9):1493–1505. [PubMed: 11290289]

Horst CJ, Johnson LV, Besharse JC. Transmembrane assemblage of the photoreceptor connecting cilium and motile cilium transition zone contain a common immunologic epitope. Cell Motil Cytoskeleton 1990;17(4):329–344. [PubMed: 1706225]

Houde C, Dickinson RJ, Houtzager VM, Cullum R, Montpetit R, Metzler M, Simpson EM, Roy S, Hayden MR, Hoodless PA, Nicholson DW. Hippi is essential for node cilia assembly and Sonic hedgehog signaling. Dev Biol 2006;300(2):523–533. [PubMed: 17027958]

Hu M, Easter SS. Retinal neurogenesis: the formation of the initial central patch of postmitotic cells. Dev Biol 1999;207(2):309–321. [PubMed: 10068465]

Huangfu D, Liu A, Rakeman AS, Murcia NS, Niswander L, Anderson KV. Hedgehog signalling in the mouse requires intraflagellar transport proteins. Nature 2003;426(6962):83–87. [PubMed: 14603322]

Kozminski KG, Johnson KA, Forscher P, Rosenbaum JL. A motility in the eukaryotic flagellum unrelated to flagellar beating. Proc Natl Acad Sci U S A 1993;90(12):5519–5523. [PubMed: 8516294]

Kramer-Zucker AG, Olale F, Haycraft CJ, Yoder BK, Schier AF, Drummond IA. Cilia-driven fluid flow in the zebrafish pronephros, brain and Kupffer's vesicle is required for normal organogenesis. Development 2005;132(8):1907–1921. [PubMed: 15790966]

Krock BL, Perkins BD. The intraflagellar transport protein IFT57 is required for cilia maintenance and regulates IFT-particle-kinesin-II dissociation in vertebrate photoreceptors. J Cell Sci 2008;121(Pt 11):1907–1915. [PubMed: 18492793]

Luby-Phelps K, Fogerty J, Baker SA, Pazour GJ, Besharse JC. Spatial distribution of intraflagellar transport proteins in vertebrate photoreceptors. Vision Res 2008;48(3):413–423. [PubMed: 17931679]

Malicki J, Neuhauss SC, Schier AF, Solnica-Krezel L, Stemple DL, Stainier DY, Abdelilah S, Zwartkruis F, Rangini Z, Driever W. Mutations affecting development of the zebrafish retina. Development 1996;123:263–273. [PubMed: 9007246]

Mendez A, Lem J, Simon M, Chen J. Light-dependent translocation of arrestin in the absence of rhodopsin phosphorylation and transducin signaling. J Neurosci 2003;23(8):3124–3129. [PubMed: 12716919]

Nawrocki, LW. Brachyodanio rerio. Institute of Neuroscience, University of Oregon; Eugene: 1985. Development of the Neural Retina in the Zebrafish.

Pazour GJ, Baker SA, Deane JA, Cole DG, Dickert BL, Rosenbaum JL, Witman GB, Besharse JC. The intraflagellar transport protein, IFT88, is essential for vertebrate photoreceptor assembly and maintenance. J Cell Biol 2002;157(1):103–113. [PubMed: 11916979]

Pazour GJ, Dickert BL, Vucica Y, Seeley ES, Rosenbaum JL, Witman GB, Cole DG. Chlamydomonas IFT88 and its mouse homologue, polycystic kidney disease gene tg737, are required for assembly of cilia and flagella. J Cell Biol 2000;151(3):709–718. [PubMed: 11062270]

Pedersen LB, Miller MS, Geimer S, Leitch JM, Rosenbaum JL, Cole DG. Chlamydomonas IFT172 is encoded by FLA11, interacts with CrEB1, and regulates IFT at the flagellar tip. Curr Biol 2005;15(3):262–266. [PubMed: 15694311]

Perkins BD, Fadool JM, Dowling JE. Photoreceptor structure and development: analyses using GFP transgenes. Methods Cell Biol 2004;76:315–331. [PubMed: 15602882]

Perkins BD, Nicholas CS, Baye LM, Link BA, Dowling JE. dazed gene is necessary for late cell type development and retinal cell maintenance in the zebrafish retina. Dev Dyn 2005;233(2):680–694. [PubMed: 15844196]

Peterson JJ, Tam BM, Moritz OL, Shelamer CL, Dugger DR, McDowell JH, Hargrave PA, Papermaster DS, Smith WC. Arrestin migrates in photoreceptors in response to light: a study of arrestin localization using an arrestin-GFP fusion protein in transgenic frogs. Exp Eye Res 2003;76(5):553–563. [PubMed: 12697419]

Raymond PA, Barthel LK, Curran GA. Developmental patterning of rod and cone photoreceptors in embryonic zebrafish. J Comp Neurol 1995;359(4):537–550. [PubMed: 7499546]

Raymond PA, Barthel LK, Rounsifer ME, Sullivan SA, Knight JK. Expression of rod and cone visual pigments in goldfish and zebrafish: a rhodopsin-like gene is expressed in cones. Neuron 1993;10(6):1161–1174. [PubMed: 8318234]

Schmitt EA, Dowling JE. Comparison of topographical patterns of ganglion and photoreceptor cell differentiation in the retina of the zebrafish, Danio rerio. J Comp Neurol 1996;371(2):222–234. [PubMed: 8835728]

Schmitt EA, Dowling JE. Early retinal development in the zebrafish, Danio rerio: light and electron microscopic analyses. J Comp Neurol 1999;404(4):515–536. [PubMed: 9987995]

Sun Z, Amsterdam A, Pazour GJ, Cole DG, Miller MS, Hopkins N. A genetic screen in zebrafish identifies cilia genes as a principal cause of cystic kidney. Development 2004;131(16):4085–4093. [PubMed: 15269167]

Tsao CC, Gorovsky MA. Different effects of tetrahymena IFT172 domains on anterograde and retrograde intraflagellar transport. Mol Biol Cell 2008;19(4):1450–1461. [PubMed: 18199688]

Tsujikawa M, Malicki J. Intraflagellar transport genes are essential for differentiation and survival of vertebrate sensory neurons. Neuron 2004;42(5):703–716. [PubMed: 15182712]

Vihtelic TS, Doro CJ, Hyde DR. Cloning and characterization of six zebrafish photoreceptor opsin cDNAs and immunolocalization of their corresponding proteins. Vis Neurosci 1999;16(3):571–585. [PubMed: 10349976]

Westerfield, M. The Zebrafish Book. Eugene, OR: University of Oregon Press; 1995.

Yoder BK, Tousson A, Millican L, Wu JH, Bugg CE Jr, Schafer JA, Balkovetz DF. Polaris, a protein disrupted in orpk mutant mice, is required for assembly of renal cilium. Am J Physiol Renal Physiol 2002;282(3):F541–552. [PubMed: 11832437]

Young RW. The renewal of photoreceptor cell outer segments. J Cell Biol 1967;33(1):61–72. [PubMed: 6033942]

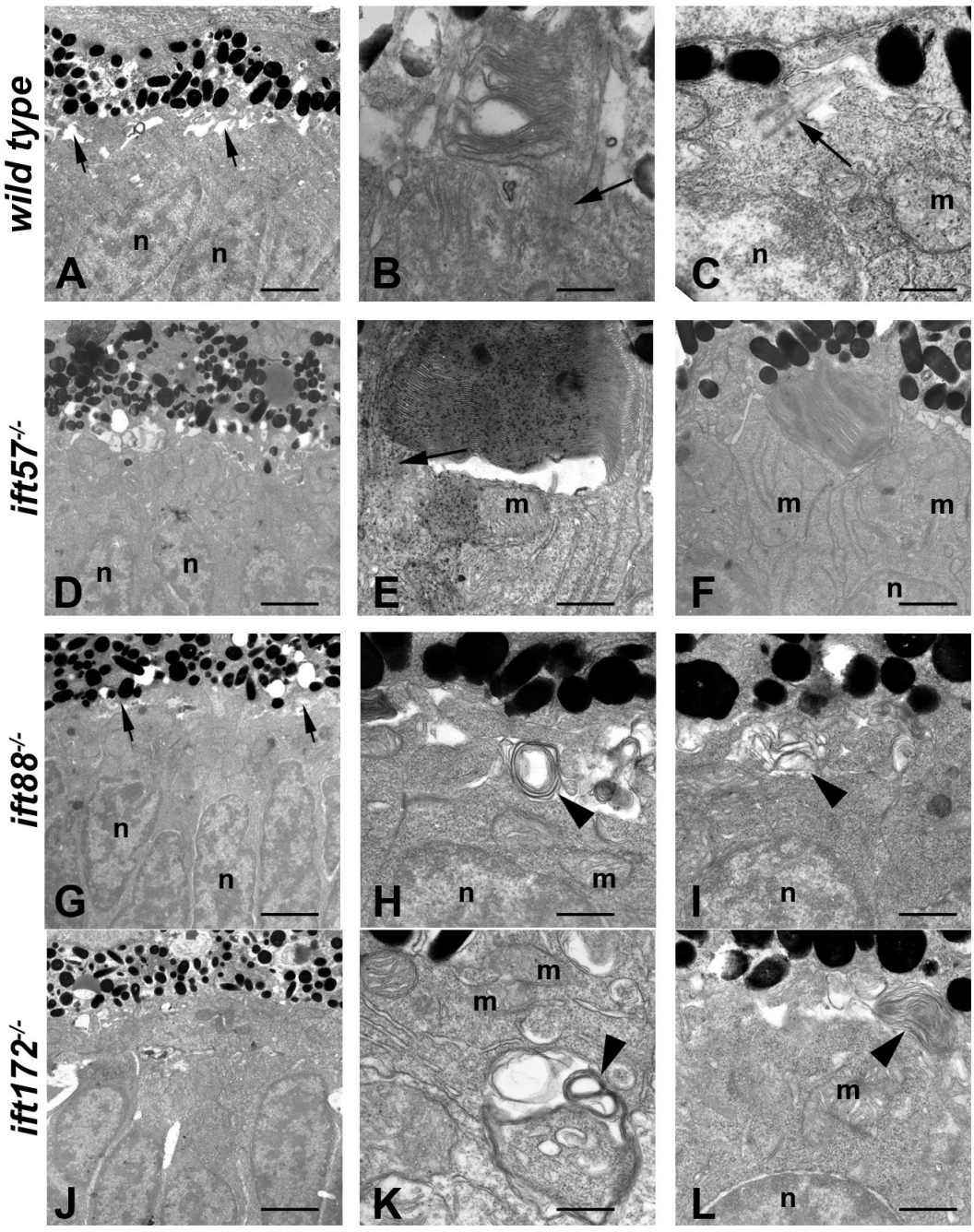

Figure 1.

Transmission electron micrographs of transverse sections along the dorsal-ventral axis of wild type, *ift57*, *ift88*, and *ift172* mutant zebrafish at 60 hpf.

A: In wild type retinas, few outer segments were observed at low magnification. The interphotoreceptor space was seen between the inner segments and the pigment epithelium (short arrows). Photoreceptor nuclei (n) were easily identified. **B, C**: At higher magnification, short outer segments with loosely organized disk membranes were seen. Connecting cilia and primitive cilia (arrows) projected from the inner segment above the mitochondria (m) and nuclei (n). **D**: *ift57* mutants appeared similar to wild type retinas at low magnification. **E, F**: High magnification of *ift57* mutants revealed outer segments with stacked disk membranes and

connecting cilia (arrow) that were located distal to the mitochondria (m) and nuclei (n). **G**: An electron micrograph of an *ift88* mutant looked similar to wild type and the interphotoreceptor space remained present (short arrows). **H, I**: Outer segments were never observed in *ift88* mutants and disorganized membrane structures (arrowheads) were seen at the apical surface of the inner segment, above the mitochondria and nuclei. **J**: A low magnification image of *ift172* mutants showed few differences from wild type. **K, L**: High magnification electron micrographs revealed disorganized membrane structures (arrowheads) located deep within the inner segment below the mitochondria (m), as well as at the apical surface. Scale bars = 4 μm (A, D, G, J), and 400nm (B, C, E, F, H, I, K, L).

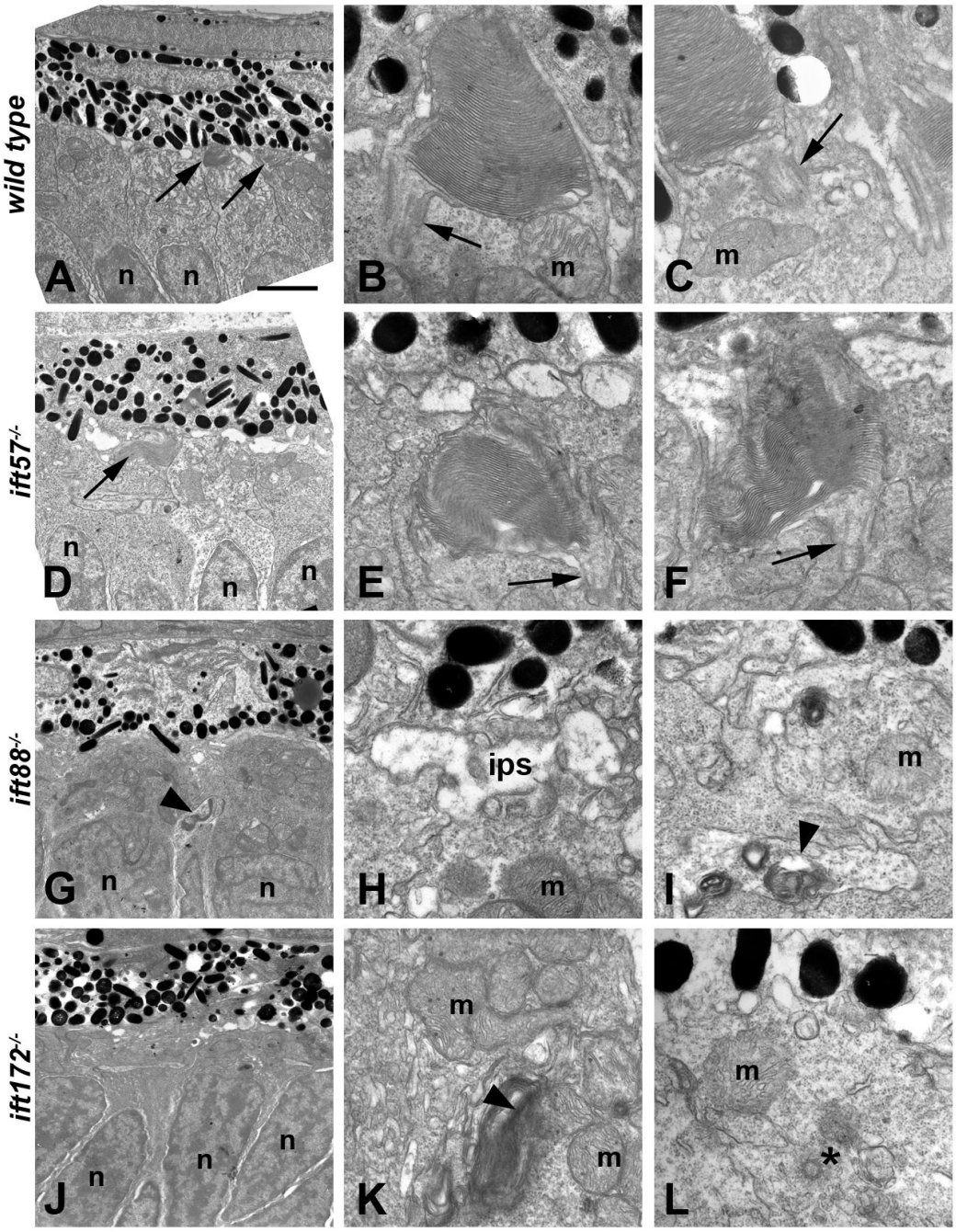

Figure 2.

Transmission electron micrographs of transverse sections along the dorsal-ventral axis of wild type, *ift57*, *ift88* and *ift172* mutant zebrafish at 72 hpf.

A: Electron micrograph of a wild type embryo showed photoreceptor outer segments (arrows) that were easily observed at low magnification. **B,C**: Higher magnification showed that outer segment disk membranes are well organized and the connecting cilium (arrows) can be seen. These cilia were approximately 300 nm in width and 500 nm in length. Mitochondria (m) were observed in the apical inner segment. **D**: In *ift57* mutants, outer segments were observed at low magnification. **E, F**: At higher magnification, the disk membranes were well ordered but the outer segments appear somewhat disheveled compared to wild type. Arrows denote connecting

cilia. **G**: In *ift88* mutants, no outer segments were seen and disorganized membrane structures (arrowhead) were seen near the nuclei (n). **H, I**: Higher magnification images revealed the interphotoreceptor space (ips) between the RPE and the mitochondria (m), as well as membrane structure (arrowheads) located basal to the mitochondria. **J**: Electron micrograph of an *ift172* mutant also showed no outer segments. **K, L**: Disorganized membrane structures (arrowhead) running parallel to the plasma membrane were seen basal to the mitochondria (m). A centriole (asterisk) that may be part of a mispositioned basal body was also seen several hundred nanometers away from the apical surface and below a mitochondria (m). Scale bar = 4 μm (A, D, G, J), and 400nm (B, C, E, F, H, I, K, L).

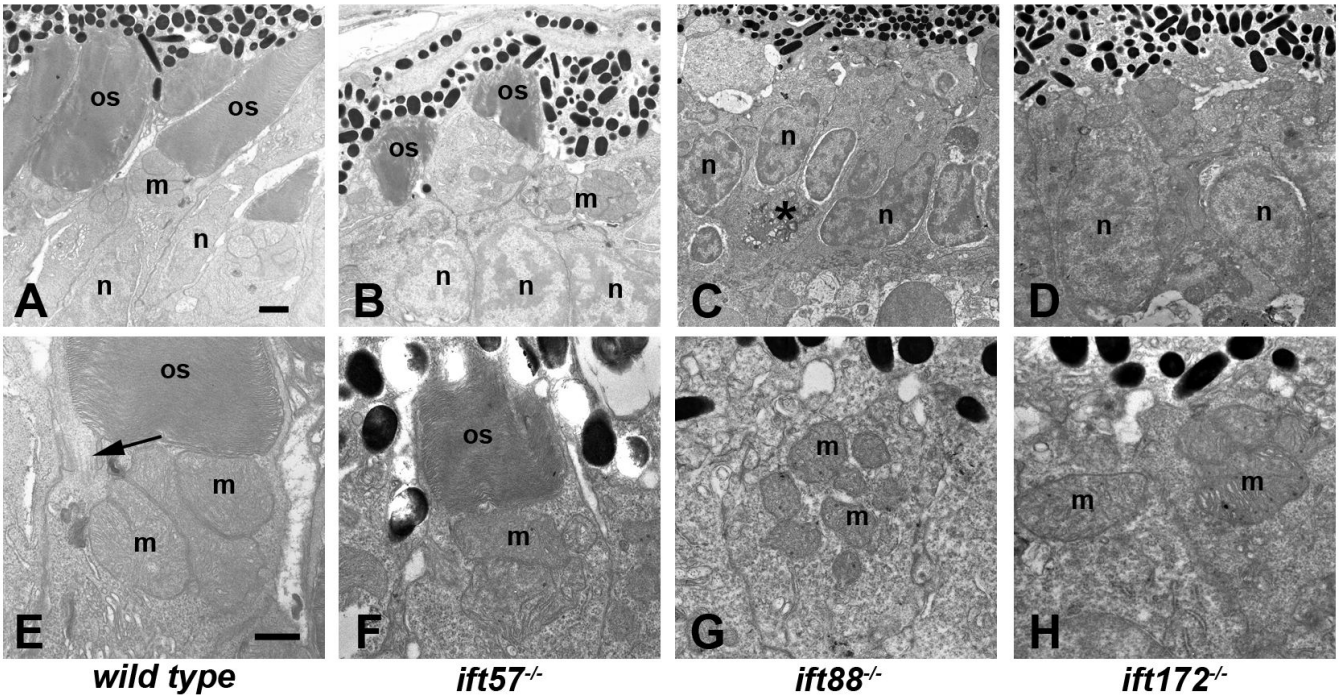

Figure 3.

Transmission electron micrographs of transverse sections along the dorsal-ventral axis of wild type, *ift57*, *ift88* and *ift172* mutant zebrafish at 96 hpf.

A-D: Low magnification images revealed longer outer segments (os) in wild type embryos. Photoreceptor outer segments were present in *ift57* mutants but were significantly shorter than wild type. Mitochondria (m) and nuclei (n) appear to be normal in the mutants. No outer segments were present in *ift88* and *ift172* mutants. Nuclei of *ift88* and *ift172* mutants were less elongated than wild type and pyknotic nuclei (asterisk, C) were occasionally observed. **E-H**: At higher magnification, the disk membranes of wild type and *ift57* mutant outer segments were highly organized. Arrow indicates connecting cilium. Numerous mitochondria (m) were seen in the apical inner segments of wild type and mutant photoreceptors. Scale bars = 1 μm (A-D), and 500 μm (E-H).

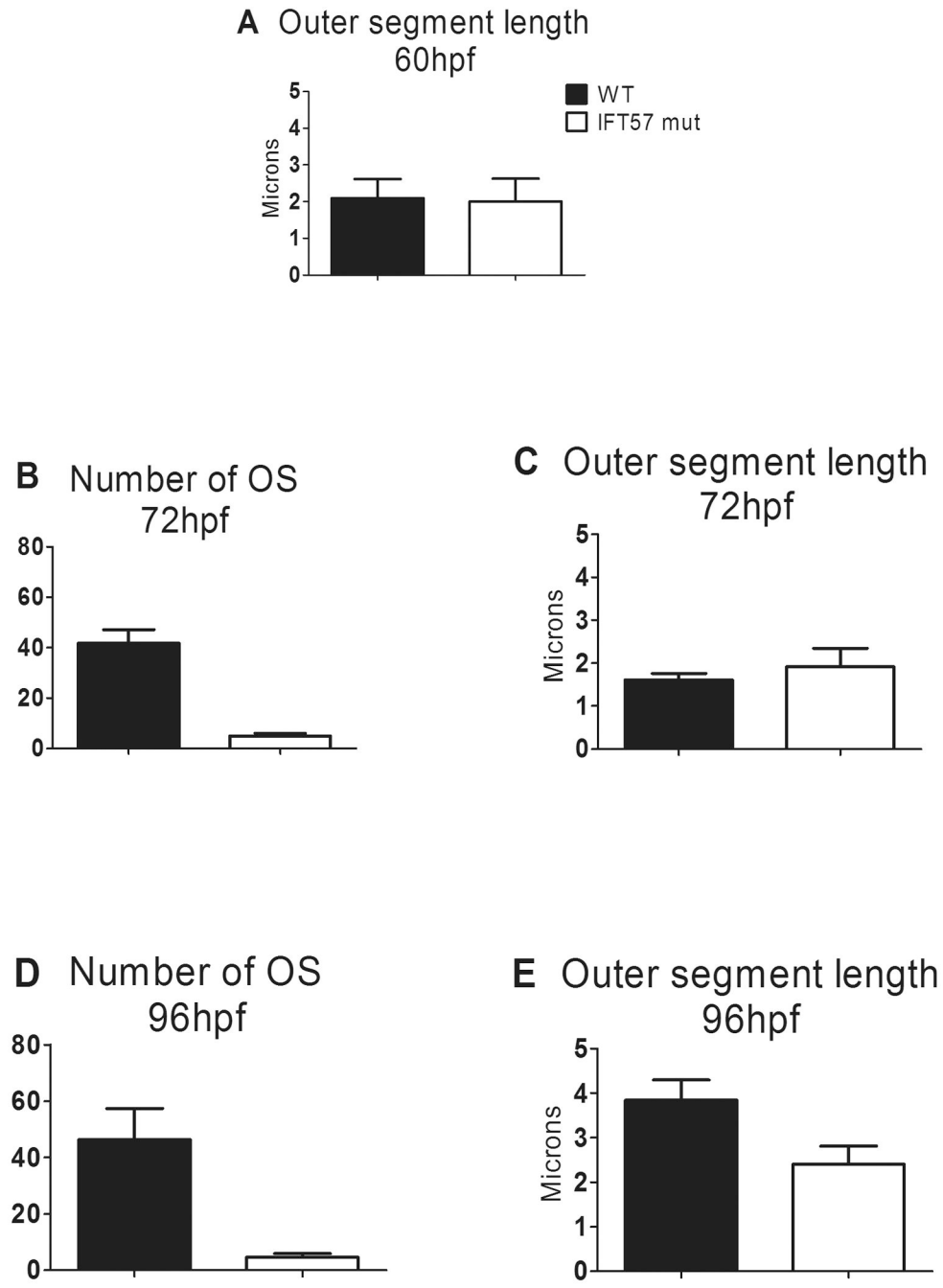

Figure 4.

Statistical analysis of the number and length of outer segments between wild type and *ift57* mutants.

A: At 60hpf, *ift57* mutants showed no difference in length when compared to wild types. **B-C**: At 72hpf, the number of outer segments in *ift57* mutant was reduced by 88% with no statistical difference in outer segment length. The length of the wild type outer segments did not significantly increase between 60 hpf and 72 hpf. **D-E**: At 96hpf, the number and length of outer segments was reduced by 90% and 38% respectively.

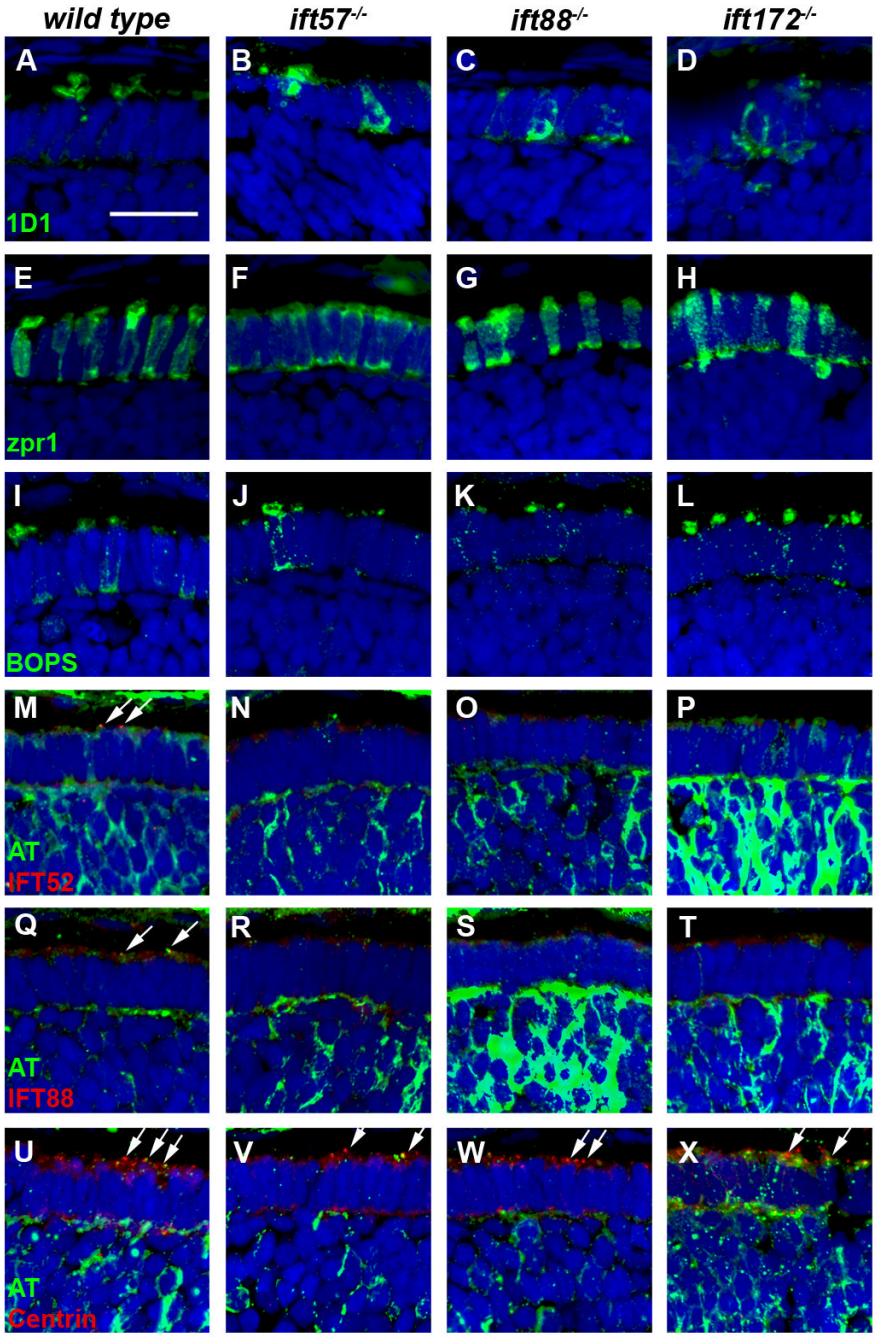

Figure 5.

Immunohistochemical analysis of wild type, *ift57*, *ift88* and *ift172* mutant zebrafish at 60 hpf. **A-D**: 1D1 (green), a marker for rhodopsin, localized to the outer segment region in wild type and *ift57* mutants. Strong mislocalization to the inner segment was also observed in *ift57* mutants, as well as *ift88*, and *ift172* mutants. **E-H**: Zpr1 (green), a label for red/green double cones gave an elongated, columnar morphology in wild type animals. Cone morphology was disheveled in the three mutants. **I-J**: Blue opsin (BOPS) was seen in small foci of wild type photoreceptors. Similar staining was seen in *ift57*, *ift88*, and *ift172* mutants. **M-P**: IFT52 (red) co-localized with acetylated tubulin (green) in the connecting cilia of wild type animals (arrows). No such staining was observed in *ift57*, *ift88* and *ift172* mutants. **Q-T**: IFT88 (red)

also showed apical localization in wild type animals (arrows). The staining partially overlapped with acetylated tubulin (green). No such staining was observed in IFT mutants. **U-X**: The basal body marker centrin (red) localized to the apical surface of the inner segment. Acetylated tubulin (green) denotes microtubules. Centrin was seen in wild type and all IFT mutants (arrows). In all images, the tissues were counterstained with DAPI (blue). Scale bar = 20 μm.

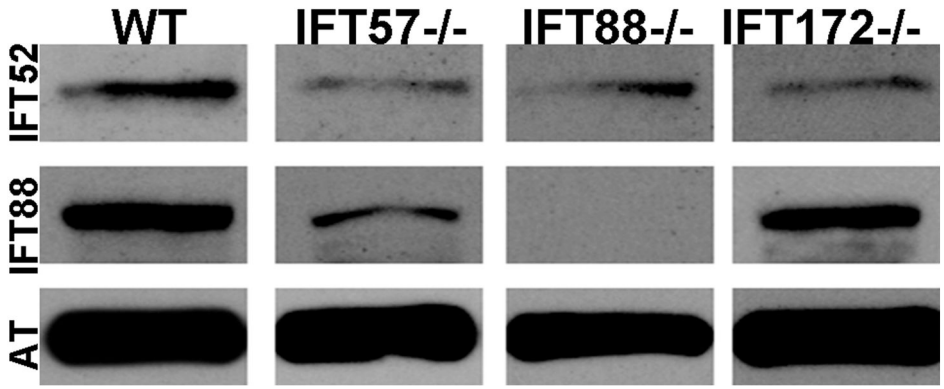

Figure 6.
Western blot analysis of whole wild type and IFT mutant embryos at 60 hpf. Immunoreactivity against IFT52 protein (top row) was detected in wild type, *ift57*, *ift88* and *ift172* mutants. Immunoreactivity against IFT88 protein (middle row) was seen only in wild type, *ift57* and *ift172* mutants, thus showing that the *ift88* mutant is null. Acetylated tubulin (AT) served as a control (bottom row).

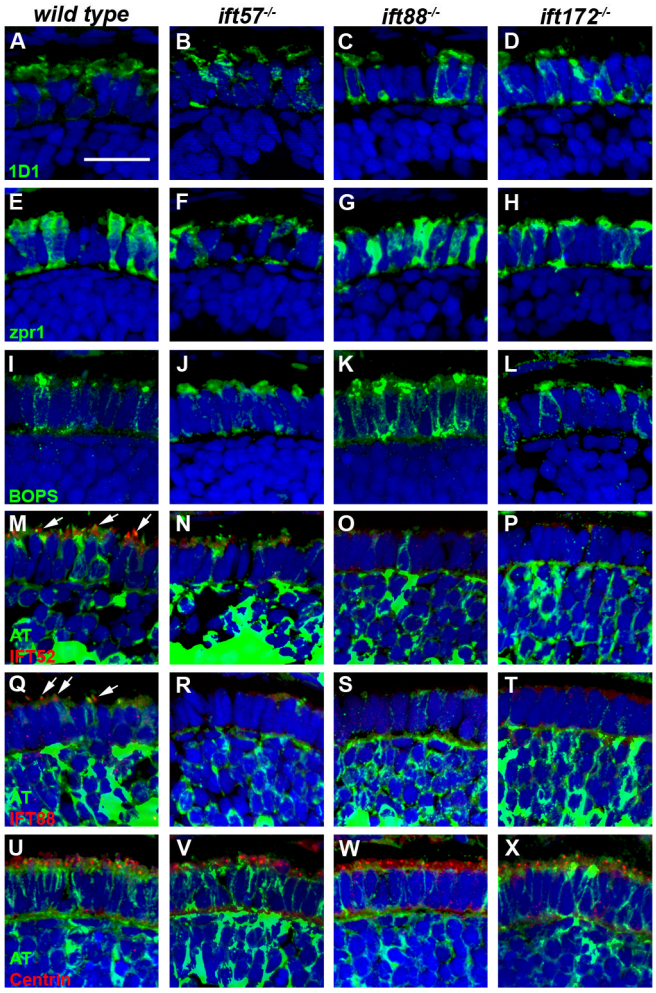

Figure 7.

Immunohistochemical analysis of wild type, *ift57*, *ift88* and *ift172* mutant zebrafish at 72 hpf. **A-D**: 1D1 (green), a marker for rhodopsin, localized to the outer segment region in wild type and *ift57* mutants. Strong mislocalization to the inner segment was observed in *ift57* mutants, as well as *ift88*, and *ift172* mutants. **E-H**: Zpr1 (green), a label for red/green double cones gave an elongated, columnar morphology in wild type animals. The columnar morphology was disrupted in the three mutants. **I-J**: Blue opsin (BOPS) was localized to putative outer segments of wild type photoreceptors, although some mislocalization was seen. Staining was observed in small the apical region of IFT mutant photoreceptors but strong mislocalization was seen in the *ift88* and *ift172* mutants. **M-P**: IFT52 (red) co-localized with acetylated tubulin (green) in the connecting cilia of wild type (arrows). No such staining was observed IFT mutants. **Q-T**: IFT88 (red) also showed strong apical localization in wild type embryos (arrows). The staining partially overlapped with acetylated tubulin (green). No staining was seen in the IFT mutants. **U-X**: The basal body marker centrin (red) localized to the apical surface of the inner segment. Acetylated tubulin (green) denotes microtubules. In all images, the tissues were counterstained with DAPI (blue). Scale bar = 20 μm.

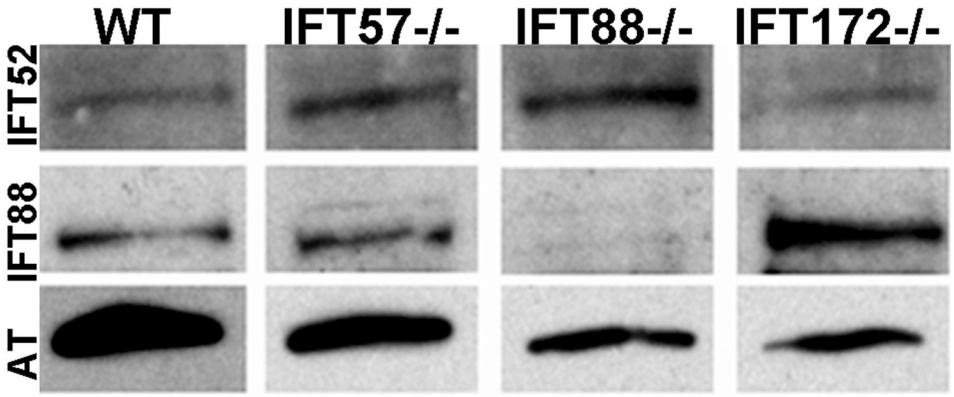

Figure 8.

Western blot analysis of whole wild type and IFT mutant embryos at 72 hpf. Immunoreactivity against IFT52 (top row) were detected in wild type and mutants at 72 hpf, confirming the expression of these subunits. IFT88 immunoreactivity (middle row) was not seen in the *ift88* mutants but continued to be expressed in other mutants as well as wild type. Acetylated tubulin (AT) served as a control (bottom row).

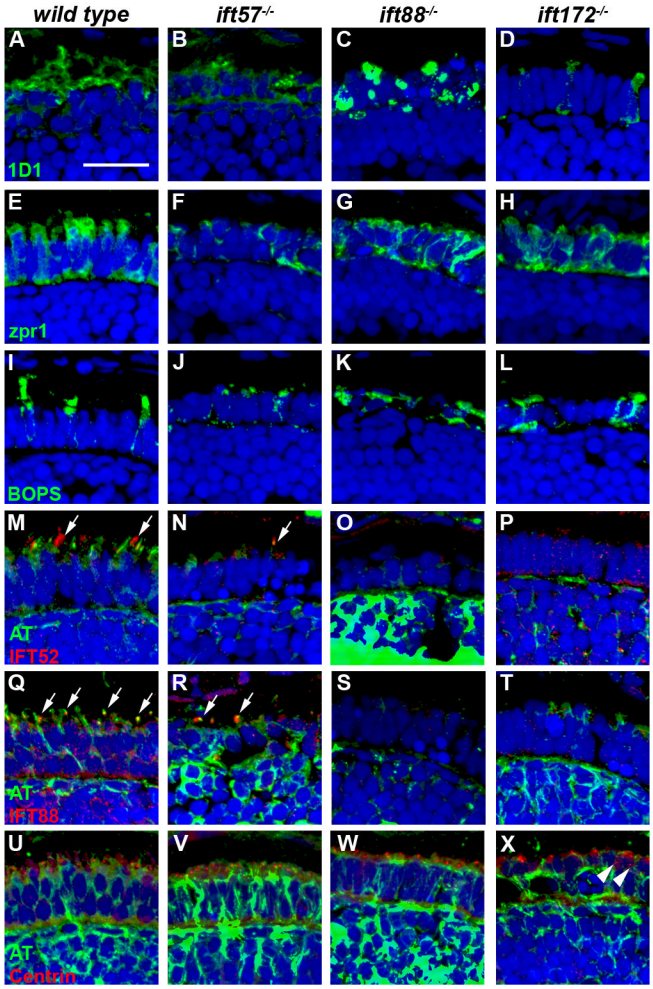

Figure 9.

Immunohistochemical analysis of wild type, *ift57*, *ift88* and *ift172* mutant zebrafish at 96 hpf. **A-D**: 1D1 (green), a marker for rhodopsin, localized to the outer segment region in wild type and *ift57* mutants. Strong mislocalization to the inner segment was also observed in *ift57*, *ift88*, and *ift172* mutants. **E-H**: Zpr1 (green), a label for red/green double cones gave an elongated, columnar morphology in wild type animals. Cone morphology was disheveled in the three mutants. **I-J**: Blue opsin (BOPS) was localized to the outer segments of wild type photoreceptors. Staining was observed in short outer segments of *ift57* photoreceptors but strong mislocalization was seen in the *ift88* and *ift172* mutants. **M-P**: IFT52 (red) co-localized with acetylated tubulin (green) in the connecting cilia of wild type and *ift57* mutants (arrows). No such staining was observed in *ift88* and *ift172* mutants. **Q-T**: IFT88 (red) also showed strong apical localization in wild type and *ift57* mutants. The staining overlapped with acetylated tubulin (green), in wild type and *ift57* animals (arrows). No staining was observed in *ift88* and *ift172* mutants. **U-X**: Centrin (red) localized to the apical surface of the inner segment. Acetylated tubulin (green) denotes microtubules. Centrin was seen in wild type and all IFT mutants. The number of centrin-positive foci was reduced in *ift88* and *ift172* mutants. Centrin was occasionally observed to be mislocalized in *ift172* mutants (Fig. 9X; white arrowheads). In all images, the tissues were counterstained with DAPI (blue). Scale bar = 20 μm.

Table 1

Comparison of photoreceptor phenotypes in zebrafish IFT mutants between 60 and 96 hpf and correlation with other ciliary defects.

	Outer segment (OS) morphogenesis			Photoreceptor-related function	Other affected tissues and functions
	60 hpf	**72 hpf**	**96 hpf**		
Wild type	Observable OS in ventral patch	More OS observed	More OS appear		
	OS ≈ 2 μm in length	No change in length	Tiering between rods and cones becoming evident		
	Loose organization of disk membranes.	Disk membranes highly ordered	OS length increased to 4 μm		
	Rhodopsin trafficking to OS	Rod and cone opsins seen in OS	Complete OS localization for rod and cone opsins		
ift57$^{-/-}$	OS phenotype similar to wild type	88% fewer OS than wild type	90% fewer OS than wild type	Not essential for OS formation and disk membrane organization	Cilia formation in C. elegans (*che-13*) (Haycraft et al., 2003)
	Mild mislocalization of rhodopsin	Length similar to wild type at ≈ 2 μm	Length increases slightly to ≈ 2.5 μm	Required for OS growth and photoreceptor survival	Kidney and nodal cilia in zebrafish and mice (Houde et al., 2006, Kramer-Zucker, Olale, Haycraft, Yoder, Schier & Drummond, 2005)
		Disk membranes organizes	More rod and cone opsins mislocalized to inner segment		Auditory and olfactory cilia formation in zebrafish (Tsujikawa & Malicki, 2004)
		Rod and cone opsins seen in OS but also mislocalization	Photoreceptors begin apoptosis		
ift88$^{-/-}$	No OS observed	No OS observed	No OS observed	Essential for primitive cilium extension and OS formation	Flagella formation in *Chlamydomonas* and *C. elegans* (Haycraft et al., 2003, Pazour et al., 2000)
	Disorganized membrane material observed in apical inner segment	Increase in number of disorganized membrane arrays	Complete mislocalization of rod and cone opsins	Not essential for basal body localization	Kidney and nodal cilia in zebrafish and mice (Kramer-Zucker et al., 2005, Yoder, Tousson, Millican, Wu, Bugg, Schafer & Balkovetz, 2002)
	Strong mislocalization of rhodopsin	Complete mislocalization of rod and cone opsins	Photoreceptors begin apoptosis		Auditory and olfactory cilia formation in zebrafish (Tsujikawa & Malicki, 2004)
ift172$^{-/-}$	No OS observed	No OS observed	No OS observed	Essential for primitive cilium extension and OS formation	Anterograde and retrograde transport in Tetrahymena and Chlamydomonas

Outer segment (OS) morphogenesis			Photoreceptor-related function	Other affected tissues and functions
60 hpf	**72 hpf**	**96 hpf**		
				flagella (Pedersen, Miller, Geimer, Leitch, Rosenbaum & Cole, 2005, Tsao & Gorovsky, 2008)
Disorganized membrane material observed in apical inner segment	Increase in number of disorganized membrane arrays	Complete mislocalization of rod and cone opsins	May play role in positioning centrioles for basal body localization	Nodal cilia formation in mice (Huangfu et al., 2003)
Strong mislocalization of rhodopsin	Complete mislocalization of rod and cone opsins	Photoreceptors begin apoptosis		
		Some mislocalization of centrin observed		